JACS
JOURNAL OF THE AMERICAN CHEMICAL SOCIETY

ARTICLE

pubs.acs.org/JACS

Non-Nernstian Two-Electron Transfer Photocatalysis at Metalloporphyrin−TiO_2 Interfaces

Shane Ardo, Darren Achey, Amanda J. Morris, Maria Abrahamsson, and Gerald J. Meyer*

Department of Chemistry and Department of Materials Science and Engineering, Johns Hopkins University, 3400 North Charles Street, Baltimore, Maryland 21218, United States

Supporting Information

ABSTRACT: A long-standing question in the photochemical sciences concerns how to integrate single-electron transfers to catalytic multielectron transfer reactions that produce useful chemical fuels. Here we provide a strategy for the two-electron formation of C−C bonds with molecular catalysts anchored to semiconductor nanocrystallites. The blue portion of the solar spectrum provides band gap excitation of the semiconductor while longer wavelengths of light initiate homolytic cleavage of metal−carbon bonds that, after interfacial charge transfer, restore the catalyst. The semiconductor utilized was the anatase polymorph of TiO_2 present as a nanocrystalline, mesoporous thin film. The catalyst was cobalt *meso*-5,10,15,20-tetrakis (4-carboxyphenyl)porphyrin chloride, Co(TCPP)Cl. For this catalyst and iron protoporphyrin IX chloride, Fe(PPIX)Cl, two distinct and sequential metal-based $M^{III/II}$ and $M^{II/I}$ reductions were observed under band gap illumination. Spectroelectrochemical characterization indicated that both reductions were non-Nernstian, behavior attributed to an environmentally dependent potential drop across the molecule−semiconductor interface. Reaction of Co^{I}(TCPP)/TiO_2 with organobromides (RBr = 1-Br-hexane or benzyl bromide) resulted in the formation of Co^{III}−R(TCPP)/TiO_2. Visible light excitation induced homolytic cleavage of the Co−C bond and the formation of C−C-bonded products. The reactions were catalytic when band gap excitation or an electrochemical bias provided TiO_2 electrons to the oxidized catalyst. Sustained photocurrents were quantified in photoelectrosynthetic solar cells under forward bias.

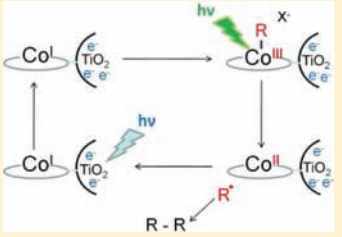

INTRODUCTION

Absorption of a single photon generally yields at most one reducing equivalent and one oxidizing equivalent.[1] How one might couple these single redox equivalents to multielectron-transfer catalysis to generate fuels has been a long-standing issue in photochemistry. The conundrum can be circumvented completely with conductive and efficient catalysts separated from light absorption in an electrolysis cell.[1−6] Another, possibly less expensive, solution is to identify assemblies that integrate light absorption, electron transfer, and catalysis via modular architectures.[7] Such assemblies would contain a component that photogenerates long-lived redox equivalents and provides them to a catalyst. Semiconductor nanocrystallites can function as this component since they have the ability to separate and store multiple charges for considerable periods of time with band gaps that can be tuned across the entire solar spectrum.[8−11] Here we report the first instance in which band gap excitation of semiconductor nanocrystallites resulted in two sequential one-electron reductions of a surface-anchored catalyst.[12−14] The emphasis was on the cobalt metalloporphyrin shown, but similar results were obtained with an iron porphyrin, Scheme 1. Photocatalysis that yielded C−C-bonded products were characterized spectroscopically and in photoelectrosynthetic solar cells.

The metalloporphyrin catalysts are known to undergo thermal $2e^-$ reduction of organohalide pollutants in fluid solution.[15−20] The catalysts were found to bind to nanocrystalline TiO_2 (anatase) mesoporous thin films, a semiconductor material widely utilized for application in light-to-electrical energy conversion in regenerative dye-sensitized solar cells. It has been estimated that about 20 trapped electrons are present in each 20 nm diameter anatase nanocrystallite at the point of maximum power conversion.[21] It is remarkable that the presence of these excess electrons is not detrimental to photoinduced electron transfer reactions under solar illumination. Indeed, the ability of the TiO_2 materials to trap and store multiple photogenerated electrons was the key feature that enabled realization of the multielectron transfer chemistry described herein. When surface anchored cobalt *meso*-5,10,15,20-tetrakis(4-carboxyphenyl)porphyrin was photoreduced to the formal oxidation state of I, Co^{I}(TCPP)/TiO_2, oxidative addition reactions with organobromides yielded Co^{III}−R/TiO_2 quantitatively. The Co−R bond was homolytically cleaved with visible light, and the catalytic state was regenerated by interfacial electron transfer from TiO_2. These reactions represent a photocatalytic $2e^-$ cycle that was quantified by transient spectroscopy and utilized to generate a photocurrent in photoelectrosynthetic solar cells. Interestingly, the redox chemistry was found to be non-Nernstian, behavior attributed to a potential drop across the semiconductor−catalyst interface.

Received: July 1, 2011
Published: September 02, 2011

Scheme 1. Structures of the porphyrins used. Left, cobalt *meso*-5,10,15,20-tetrakis(4-carboxyphenyl)porphyrin. Right, iron protoporphyrin IX

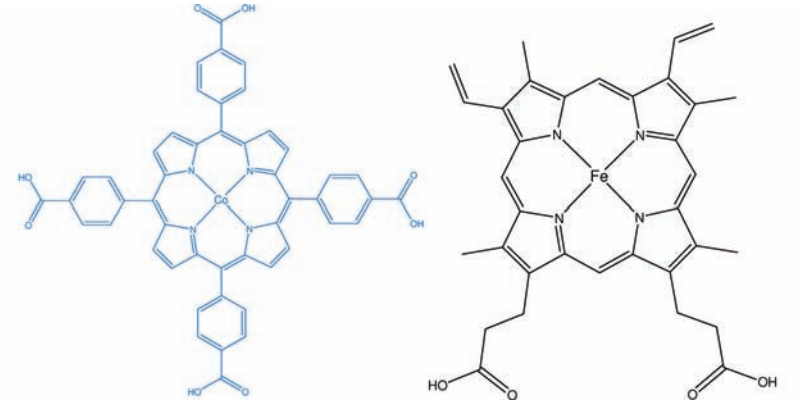

EXPERIMENTAL SECTION

Materials. The following reagents and substrates were used as received from the indicated commercial suppliers: acetonitrile (Burdick & Jackson, spectrophotometric grade); methanol (Sigma-Aldrich, spectrophotometric grade, > 99.9%); dimethylsulfoxide (DMSO; Fisher Scientific, 99.9%); pyridine (py; Burdick & Jackson, 99.9%); deionized water; acetone (bulk solvent); lithium perchlorate (Aldrich, 99.99%); tetra-*n*-butylammonium perchlorate ($TBAClO_4$; Fluka, > 99.9%); tetra-*n*-butylammonium hexafluorophosphate ($TBAPF_6$; Fluka, > 99.0%); tetra-*n*-butylammonium borohydride ($TBABH_4$; Aldrich, 98%); tetra-*n*-butylammonium hydroxide (TBAOH; Fluka, 1 M aqueous); potassium hydroxide (Fisher Scientific, 87.2%); lithium hydroxide (Aldrich, 98+ %); hydrochloric acid (Fisher Scientific, 37.2% aqueous solution); 1-bromohexane (Aldrich, 98%); benzyl bromide (Aldrich, 98%); cobalt(III) *meso*-5,10,15,20-tetrakis(4-carboxyphenyl)porphyrin chloride (Frontier Scientific); iron(III) protoporphyrin IX (Fisher Scientific); argon gas (Airgas, > 99.998%); oxygen gas (Airgas, industrial grade); titanium(IV) isopropoxide (Sigma-Aldrich, 97%); fluorine-doped SnO_2-coated glass (FTO; Hartford Glass Co., Inc., 2.3 mm thick, 15 Ω/□); and glass microscope slides (Fisher Scientific, 1 mm thick).

Preparations. *Sensitized Metal-Oxide Thin Film (Electrode).* Transparent TiO_2 nanocrystallites (anatase, ∼ 15 nm in diameter) were prepared by hydrolysis of Ti(*i*-OPr)$_4$ using a sol−gel technique previously described in the literature.[22] The sols were cast as mesoporous thin films, using Scotch transparent film tape as a spacer (∼ 10 μm thick), by doctor blading onto glass microscope slides for spectroscopic measurements and transparent FTO conductive substrates for electrochemical measurements. In all cases, the thin films were annealed at 420 °C for 30 min under an atmosphere of O_2 flow.

The thin films were first pretreated with aqueous base (pH 11) for 15 min, followed by an acetone wash and drying at 75 °C. The films were then briefly immersed in neat DMSO and then transferred to a DMSO solution that contained μM concentrations of the catalysts. Within an hour, the film became darkly colored. Films were then immersed in neat DMSO for 5−10 min followed by a thorough washing with CH_3CN. These metalloporphyrin TiO_2 thin films were positioned in a standard 1 cm^2 quartz cuvette containing the experimental solution. The cuvettes containing the thin film and electrolyte solution were purged with Ar(g) for at least 30 min prior to experimentation. The macroscopic surface coverage, Γ, in mol/cm^2, was determined from the measured absorption with the modified Beer−Lambert law formula of eq 1,

$$\text{Abs} = 1000 \times \Gamma\varepsilon \qquad (1)$$

where ε is the molar decadic extinction (absorption) coefficient, $M^{-1}\,cm^{-1}$, that was assumed to be the same in solution and on the surface. The metalloporphyrins were typically anchored to the thin films at surface coverages of $\Gamma \approx 1-4 \times 10^{-9}$ mol/cm^2, which are <10% of the saturation values.

Experimental Solution Compositions. For spectroscopy experiments, sensitized TiO_2 thin films were immersed in argon-purged acetonitrile with pyridine (500:1, v/v). For electrochemical and spectroelectrochemical experiments, 100 mM $LiClO_4$, $TBAClO_4$, or $TBAPF_6$ electrolyte solutions in argon-purged acetonitrile/pyridine (500:1, v/v) were utilized.

Spectroscopy. Steady-state UV−visible (vis) absorption spectra were obtained on a Varian Cary 50 spectrophotometer at room temperature. For some experiments, the absorption spectra were recorded under steady-state white-light illumination from a 150 W Xe arc lamp employing various long pass filters to control the rate of photoreduction.

Nanosecond transient absorption measurements were obtained with an apparatus similar to that which has been previously described.[24] Briefly, samples were excited by a Q-switched, pulsed Nd:YAG laser (Quantel USA (BigSky) Brilliant B; 5−6 ns full width at half-maximum (fwhm), 1 Hz, ∼10 mm in diameter) directed 45° to the film surface and through the FTO side for films supported on FTO tuned to 532 nm with the appropriate nonlinear optics. The excitation fluence was measured by a thermopile power meter (Molectron) and was <6 mJ/cm^2 so that the absorbed fluence was typically ≤1 mJ/cm^2. A Glan−Taylor polarizer was employed in the laser path to attenuate the pulse fluence. A 150 W xenon arc lamp served as the probe beam (Applied Photophysics) and was aligned orthogonal to the laser excitation light. Before arriving at the sample, this probe beam was directed through a 1/4 m monochromator (Spectral Energy, Corp. GM 252) to lessen the effects of probe-beam photoexcitation. For detection at sub-100 microsecond time scales the lamp was pulsed with 100 V. Detection was achieved with a monochromator (Spex 1702/04) optically coupled to an R928 photomultiplier tube (Hamamatsu). Transient data were acquired on a computer-interfaced digital oscilloscope (LeCroy 9450, Dual 350 MHz) with 2.5 ns resolution terminated at 50 Ω for sub-100 μs data acquisition; for longer time scales, the signal was terminated with a 10 kΩ resistor and bandwidth limited at 80 MHz. The overall instrument response time was ∼10 ns. Typically, 15−30 laser pulses were averaged at each observation wavelength over the range 360−500 nm, at 10 nm intervals. Full spectra were generated by averaging multiple data points. Quantum yields were determined on the basis of the irradiance of the incoming light measured by a thermopile power meter corrected for the absorptance of the sample, relative to the magnitude of the transient absorption changes converted to coverage by eq 1.

Electrochemistry. A potentiostat (BAS model CV-50W or Epsilon electrochemical analyzer) was employed for measurements in a standard

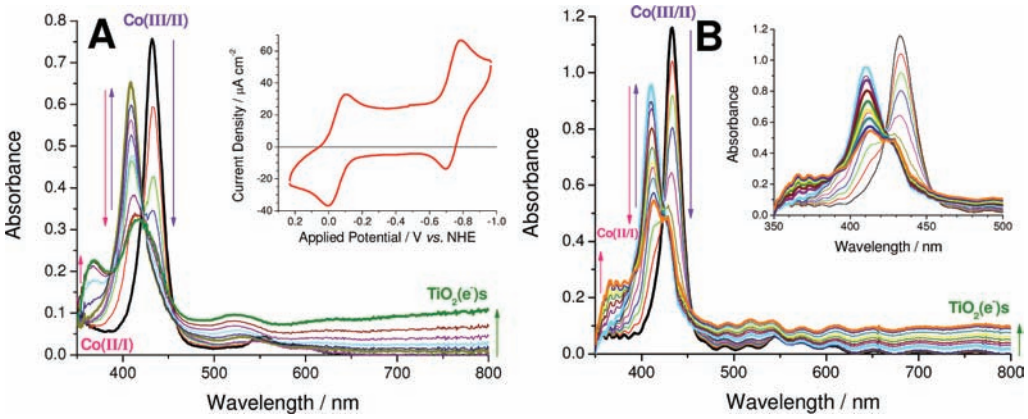

Figure 1. (A) Absorption spectra recorded for a Co(TCPP)/TiO_2 thin-film electrode immersed in the standard electrolyte containing 100 mM $LiClO_4$ as the Fermi level was raised from 0.0 V to −1.0 V vs NHE. The inset displays a cyclic voltammogram of Co(TCPP)Cl in Ar-purged 100 mM $TBAClO_4$/DMSO-pyridine. (B) Absorption spectra for a Co(TCPP)/TiO_2 thin film immersed in the same electrolyte as in (A) but with methanol (2%, v/v) recorded under steady-state white-light illumination from a 150 W Xe arc lamp. The inset is an expanded version of the 350−500 nm data.

three-electrode arrangement with a glassy carbon disk or sensitized TiO_2 thin film deposited on an FTO substrate working electrode, a Pt gauze or Pt disk (Bioanalytical Scientific Instruments, Inc.) counterelectrode, and an aqueous Ag/AgCl (KCl saturated) reference electrode (Bioanalytical Scientific Instruments, Inc.). All potentials are reported versus the normal hydrogen electrode (NHE) unless otherwise noted. The ferrocenium/ferrocene ($Fe(Cp)_2^{+/0}$) half-wave potential was measured both before and after each experiment in a 200 mM $LiClO_4$/acetonitrile electrolyte and was used as a standard to calibrate the reference electrode. Conversion to vs NHE was achieved correcting for the expected $E_{1/2}(Fe(Cp)_2^{+/0})$ of +310 mV vs the KCl-saturated aqueous calomel electrode (SCE), where SCE is +241.2 mV vs NHE.[25]

Spectroelectrochemistry was performed via application of a potential bias concurrent with monitoring the UV−vis absorption spectra of sensitized TiO_2 thin-film electrodes immersed in the standard electrolytes. At each potential step, a spectrum that was invariant with time was recorded, and the process was repeated. Single-wavelength absorption features plotted as a function of potential bias were proportional to the cumulative formation/loss of states; for the $TiO_2(e^-)$ absorption features this was directly related to the cumulative TiO_2 density of states in free energy.

Mass Spectrometry. Gas chromatography (GC) mass spectrometry (MS) measurements were obtained on a GC-17A instrument (Shimadzu Scientific Instruments) coupled to a GCMS-QP5050A detector (Shimadzu Scientific Instruments), set at 1.5 kV. The column was DB-5 ms (Agilent Technologies) which consisted of a nonpolar, phenyl arylene polymer and was 30 m in length, 0.25 μm thick, and 0.25 mm in diameter. Samples were injected (∼0.1 μL) into a preheated injection port (220 °C) via an autosampler and separated by a custom temperature-ramp program, as follows: 50 °C (held for 5 min); 5 °C/min to 70 °C; 20 °C/min to 290 °C (held for 5 min).

Data Fitting. Kinetic data fitting and spectral modeling were performed in Origin 7.0, and least-squares error minimization was accomplished using the Levenberg−Marquardt iteration method. Values are reported as means with standard error of the final digit in parentheses. For the spectral modeling, a method for the standard addition of known spectra was developed using the C programming language and was implemented in Origin's error minimization routine.

RESULTS

Shown in Figure 1A are representative spectra recorded for Co(TCPP) anchored to a mesoporous, nanocrystalline TiO_2 (anatase) thin-film electrode, abbreviated Co(TCPP)/TiO_2, at different applied potentials, where TCPP is *meso*-5,10,15,20-tetrakis(4-carboxyphenyl)porphyrin. As the Fermi level of the functionalized TiO_2 film was raised toward the vacuum level, spectral changes associated with the following redox processes were sequentially observed: (1) the metalloporphyrin was reduced from Co^{III} to Co^{II} with maintenance of isosbestic points; (2) partial reduction of TiO_2 to yield $TiO_2(e^-)$; and (3) Co^{II} was reduced to Co^{I} concomitant with an increase in $[TiO_2(e^-)]$. The spectral assignments were based upon those previously reported.[26−29] When the Fermi level was lowered, steps 1−3 were sequentially reversed and the initial Co^{III}-(TCPP)/TiO_2 was restored. Band-gap excitation of a Co^{III}-(TCPP)/TiO_2 thin film in acetonitrile containing methanol (2%, v/v) as a sacrificial donor resulted in the same reactions 1−3, Figure 1B. In fluid DMSO solution with an excess of pyridine on a per molar basis, two quasi-reversible waves were observed in a cyclic voltammetry experiment, Figure 1A inset.

Table 1. Visible Absorption Properties for the Soret Band of Co(TCPP) and Fe(PPIX)

	absorption maxima, nm (ε, 10^5 M^{-1} cm^{-1})		
	M^{III}	M^{II}	M^{I}
Co(TCPP)/TiO_2/CH_3CN	432 (2.5)	410 (2.1)	416 (1.1); 366 (0.7)
Fe(PPIX)/DMSO	396 (1.4)	423 (3.2)	488 (0.6)
Fe(PPIX)/Py	398 (1.4)	419 (3.3)	488 (0.4)

The same series of reactions 1−3 were observed in the electro- and photochemical reduction of Fe^{III}(PPIX)/TiO_2 in DMSO and pyridine electrolytes, where PPIX is protoporphyrin IX. A complication with the heme electrochemistry was that the $Fe^{III/II}$ process was not precisely determined due to a competitive autoreduction process.[30] Nevertheless, the reduction of Fe^{II} to Fe^{I} was observed under forward bias, and both $Fe^{III/II}$ and $Fe^{II/I}$ redox processes were quantified under band gap illumination. A summary of the spectroscopic properties is shown in Table 1.

Figure 2 presents absorption changes measured as a function of applied potential at 373 and 950 nm. The data recorded at 950 nm was solely due to changes in the $TiO_2(e^-)$ concentration,

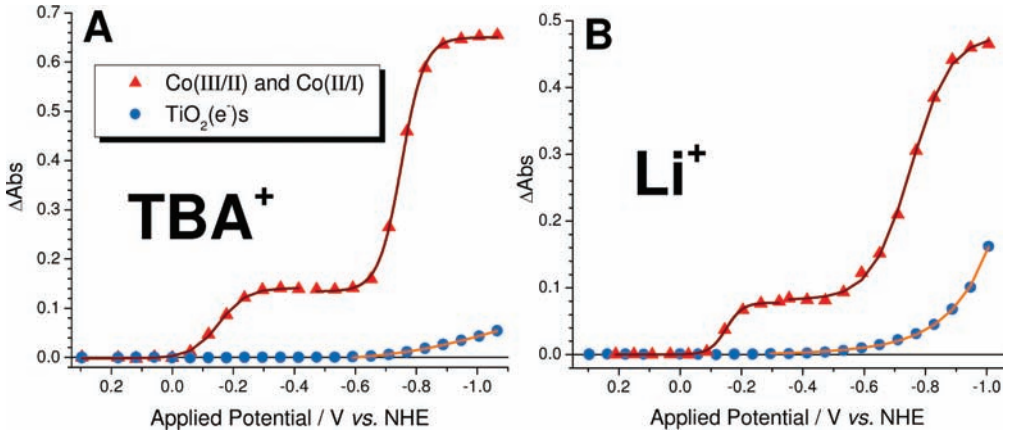

Figure 2. Absorbance changes measured at 373 nm (red triangles) as a function of applied potential for a Co(TCPP)/TiO_2 thin-film electrode immersed in the standard electrolyte with 100 mM (A) $TBAClO_4$ or (B) $LiClO_4$. Also shown are the absorbance values at 950 nm (blue circles) which represent the concentration of $TiO_2(e^-)$ overlaid with a fit to an exponential function.

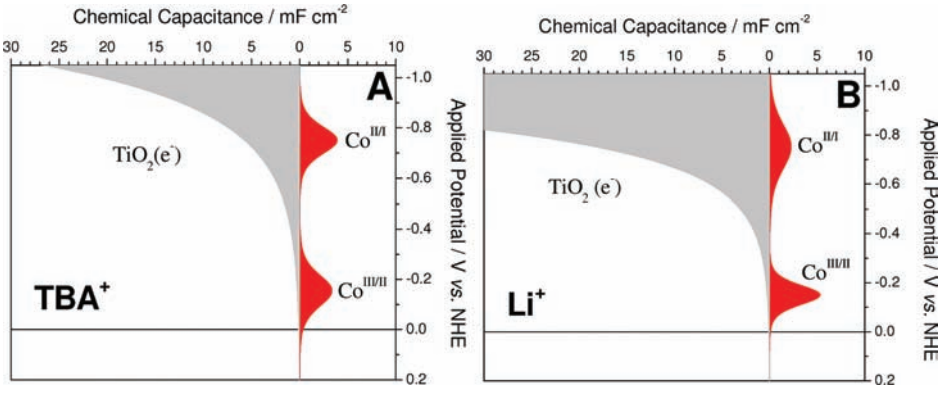

Figure 3. Chemical capacitance for a Co(TCPP)/TiO_2 thin-film electrode immersed in the standard electrolyte with 100 mM (A) $TBAClO_4$ or (B) $LiClO_4$, for $Co^{III/II}$, $Co^{II/I}$, and $TiO_2(e^-)$ as a function of applied potential.

while the 373 nm wavelength represents a $TiO_2(e^-)$ isosbestic point, and the changes measured there were representative of only the Co(TCPP) oxidation state changes. Small amounts of degradation and desorption of Co^I(TCPP) from the surface was observed when the applied potentials were held at negative values for extended periods. Therefore, this was avoided. To ensure that desorption and degradation did not significantly impact the data, after each cathodic excursion the potential was stepped back to the initial value, and the final absorbance spectrum was compared with the initial one.

At room temperature, these cobalt reduction processes did not follow the Nernst equation, eq 2,

$$E = E^0 - \frac{59\ \text{mV}}{n} \log_{10}\left(\frac{[\text{red}]}{[\text{ox}]}\right) \quad (2)$$

when E_{app}, the applied potential, was used in place of E and E^0 is the formal reduction potential. Therefore, an ideality factor, a, was integrated into the prelogarithmic term, that with rearrangement led to eq 3,

$$x = \frac{1}{1 + 10^{E_{app} - E^0/a \times 59\ \text{mV}}} \quad (3)$$

where x is the fraction of catalyst present in the reduced redox state. Equation 3 modeled the sequential sigmoidal shapes due to conversion from Co^{III} to Co^{II} and from Co^{II} to Co^{I} successfully and is superimposed on the data in Figure 2. The absorbance due to $TiO_2(e^-)$ is shown as dark blue dots and is overlaid with a fit to an exponential function.

The spectroelectrochemical data are most easily understood by fitting the distributions shown in Figure 2 to eq 3 and then taking their derivatives,[31−33] as plotted in Figure 3. The same analysis for Fe(PPIX)/TiO_2 is shown in Figure S1 (Supporting Information). Murray has suggested the term 'chemical capacitance' that we adopt here with units of mF/cm^2.[31] The ideality factors and the reduction potentials, taken as the potentials where the concentrations of the two redox states were equal, are given in Table 2.

The ideality factors measured in TBA^+-containing electrolytes were approximately the same for the $Co^{III/II}$ and $Co^{II/I}$ redox processes. However, when $LiClO_4$ was employed, the $Co^{III/II}$ ideality factor was always $\leq$1.6 and typically close to unity. The ideality factor for $Co^{II/I}$ was consistently larger, $1.6 \leq a \leq 2.5$, when the $TiO_2(e^-)$ concentration was the largest. The percentage of the applied potential that dropped across the redox center, S, was calculated with the determined ideality factors through eq 4.

$$S = \frac{a - 1}{a} \times 100\% \quad (4)$$

dx.doi.org/10.1021/ja206139n |J. Am. Chem. Soc. 2011, 133, 16572–16580

Table 2. Metalloporphyrin/TiO_2 Reduction Potentials, E^0, and Ideality Factors, *a*

	$M^{III/II}$		$M^{II/I}$	
TiO_2 conditions	E^0/V	*a*	E^0/V	*a*
Co(TCPP) $LiClO_4/CH_3CN$/Py	-0.09 ± 0.01	1.2 ± 0.2	-0.72 ± 0.01	1.8 ± 0.2
Co(TCPP) $TBAClO_4/CH_3CN$/Py	-0.31 ± 0.03	1.9 ± 0.1	-0.77 ± 0.02	1.9 ± 0.4
Co(TCPP) $TBAClO_4$/DMSO/Py	-0.05^a	–	-0.74^a	–
Fe(PPIX) $TBAPF_6$/DMSO	-0.16^a	–	-1.07	1.6

[a] Measured as $E_{1/2}$ values in fluid solution via cyclic voltammetry at 20 and 100 mV/s at a glassy carbon disk electrode. The redox chemistry was quasi-reversible.

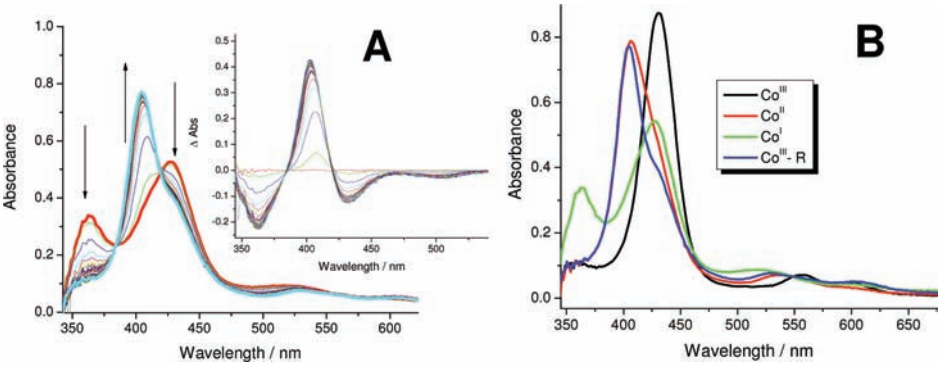

Figure 4. (A) UV−visible absorption spectra measured after the introduction of 1-bromohexane to a $Co^I(TCPP)/TiO_2(e^-)$ thin film immersed in the standard TBA^+ electrolyte. Vertical arrows indicate the absorption change over time. Inset displays absorption difference spectra measured when the initial $Co^I(TCPP)/TiO_2(e^-)$ absorption spectrum was used as a reference. (B) Absorption spectra of the indicated Co(TCPP)/TiO_2 species in the standard TBA^+ electrolyte.

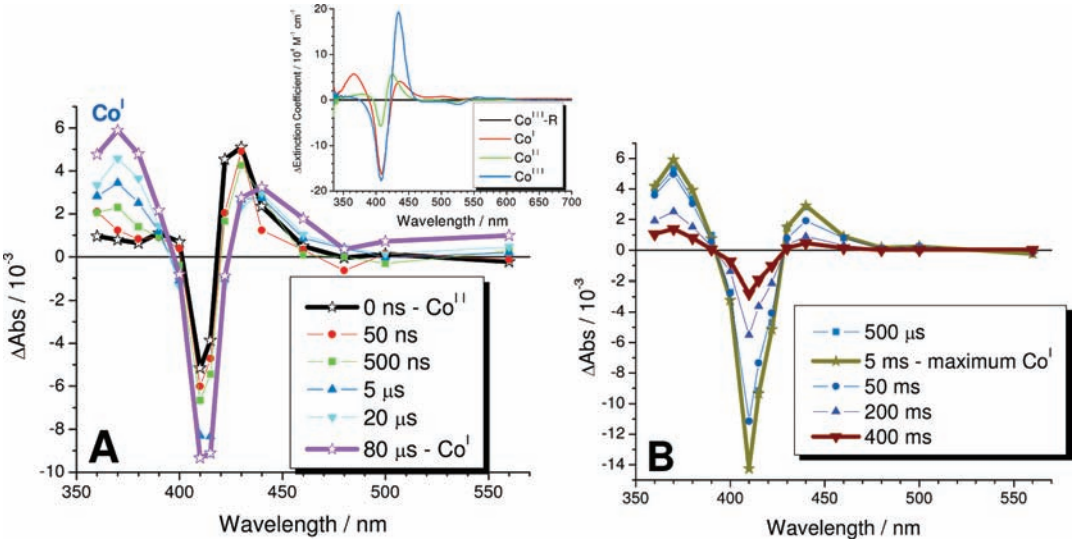

Figure 5. (A) Transient absorption difference spectra measured at the indicated delay times after pulsed 532 nm excitation of a $Co^{III}-R/TiO_2(e^-)$ thin-film electrode immersed in the standard TBA^+ electrolyte with 1-bromohexane (10%, v/v, 0.7 M) and biased to −810 mV vs NHE. Prompt formation of Co^{II} was observed followed by reduction of Co^{II} to Co^I by $TiO_2(e^-)$. Inset depicts the extinction coefficient spectra with a $Co^{III}-R/TiO_2(e^-)$ reference. (B) The same as in panel A but at longer delay times that highlight the slow reaction of Co^I with 1-bromohexane to yield $Co^{III}-R$.

Analysis in $LiClO_4$ found fractional potential drops of only ~15% for the $Co^{III/II}$ couple, yet noticeably larger for the $Co^{II/I}$ couple, ~45%. The ideality factors and hence applied potential drops were found to be invariant to the surface coverage of the metalloporphyrins over the range of surface coverages studied ($\sim 1 \times 10^{-10} - 4 \times 10^{-9}$ mol/cm^2).

The reaction of a variety of organohalides with a $Co^ITCPP/TiO_2(e^-)$ thin-film electrode resulted in absorption changes consistent with formation of a carbon−cobalt bond.[15,16] The reactivity of 1-bromohexane ($1\text{-}BrC_6H_{13}$), and benzyl bromide ($Br-C_7H_7$) were studied in the most detail. The addition of excess 1-bromohexane to the external acetonitrile electrolyte

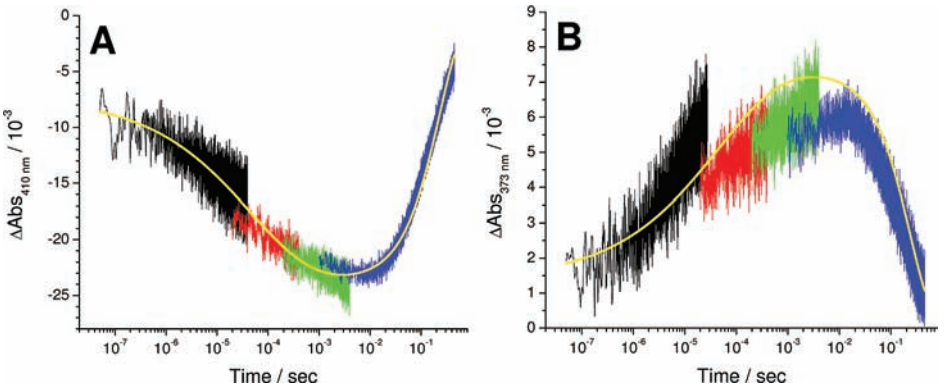

Figure 6. (A) Transient absorption differences measured at 410 nm after pulsed 532 nm excitation for the sample in Figure 5. Overlaid is a kinetic fit to the sum of a first-order process, k_{obs} = 4.26(3) s^{-1} and stretched-exponential function, k = 2.2(2) × 10^4 s^{-1} with β = 0.365 based on fits to eq 5. (B) Transient absorption differences measured at 373 nm after pulsed 532 nm excitation for the sample in Figure 5, overlaid with a kinetic fit (yellow line). All kinetic parameters from panel A were employed, except that the initial and maximum amplitudes were scaled by the ratio of the absorptions at 373 and 410 nm for Co^{II}, initial, and Co^{I}, maximum, using the data from the inset to Figure 5a.

surrounding a $Co^{I}(TCPP)/TiO_2(e^-)$ thin film resulted in UV−visible absorption changes consistent with a quantitative reaction to yield $Co^{III}-C_6H_{13}(TCPP)/TiO_2(e^-)$ with maintenance of isosbestic points, Figure 4A. The $Co^{III}-C_6H_{13}(TCPP)/TiO_2(e^-)$ was stable and displayed only the slow loss of the long wavelength absorption characteristic of $TiO_2(e^-)$. Once all the $TiO_2(e^-)$ had reacted, the $Co^{III}-C_6H_{13}(TCPP)/TiO_2$ was stable in the dark for ~30 min as judged by UV−vis spectroscopy. Hence, the formation of the organometallic product prevented further reaction.

Visible-light excitation of $Co^{III}-R(TCPP)/TiO_2(e^-)$ resulted in a photochemical reaction. Transient absorption difference spectra measured after pulsed 532 nm laser excitation of a $Co^{III}-R/TiO_2(e^-)$ thin-film electrode, where R = hexyl, are displayed in Figure 5A. The spectrum observed immediately after laser excitation was within experimental error the same as that of $Co^{II}(TCPP)/TiO_2(e^-)$, formed with a quantum yield of 0.15 ± 0.05. The $Co^{II}(TCPP)/TiO_2(e^-)$ intermediate was subsequently reduced to Co^{I} by $TiO_2(e^-)$ on the nano- to millisecond time scale, Figure 5. The transient data for this process were not first-order but could be adequately fit to the Kohlrausch−Williams−Watts (KWW) kinetic model,[34,35] eq 5, with β fixed at 0.365,

$$\Delta Abs(t) = \Delta Abs_0 \exp[-(kt)^{\beta}] \quad (5)$$

where β is inversely related to the width of the underlying Lévy distribution of rate constants, $0 < \beta < 1$, and k is a characteristic rate constant.[36] On the basis of multiple measurements and spectral modeling it was concluded that Co^{II} was reduced to Co^{I} with a quantum yield greater than 0.85. A lower limit was set due to the possibility that some Co^{I} + 1-bromohexane reacted over the course of the Co^{II} to Co^{I} transformation. The $Co^{I}(TCPP)/TiO_2(e^-)$ was then found to react with 1-bromohexane by first-order kinetics, Figure 6. The same reactions were observed when the organohalide employed was benzyl bromide.

With knowledge of extinction coefficients and the fitting parameters obtained from the fits in Figure 6A, the transient absorption differences measured at 373 nm as shown in Figure 6B were also well described by the same kinetic models. Plots of the observed pseudo-first-order rate constants, k_{obs}, obtained from the second portion of the fits yielded a second-order rate

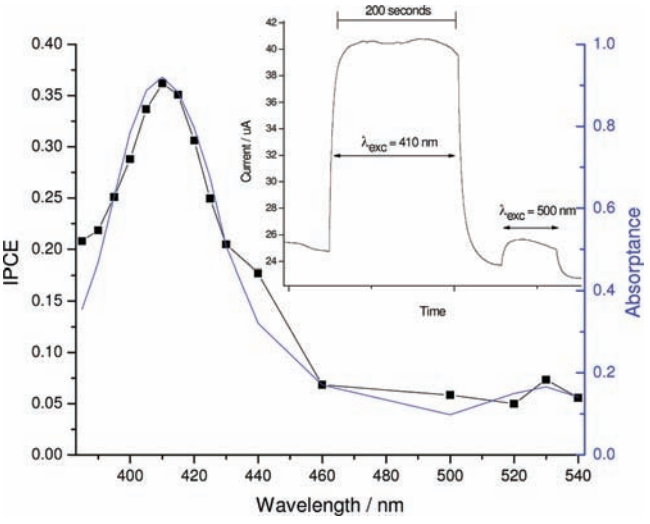

Figure 7. Photocurrent action (black) and absorptance (blue) spectra of a $Co(TCPP)/TiO_2$ thin film immersed in the standard TBA^+ electrolyte with 0.7 M 1-bromohexane at an applied potential of −880 mV vs NHE. Inset depicts photocurrents measured with the indicated excitation wavelengths on an ~1 cm^2 $Co(TCPP)/TiO_2$ thin film.

constant for the reaction with 1-bromohexane, $k_2 \approx 6$ M^{-1} s^{-1}. The same analysis was performed with benzyl bromide and resulted in $k_2 \approx 250$ M^{-1} s^{-1}.

In the presence of a sacrificial donor (methanol), photolysis from a 150 W Xe lamp allows for ultraviolet bandgap excitation in conjunction with visible light-initiated photodissociation to incur the catalytic reduction of benzyl bromide by $CoTCPP/TiO_2(e^-)$. This full photocatalytic cycle occurred 400−550 times per catalyst before degradation, on the basis of the concentration of bibenzyl formed. Although stable over the course of hours under constant photolysis, a side reaction was spectrally observed, consistent with that previously assigned as alkyl migration from the cobalt center to the pyrrole nitrogen, Co−N−R.[37] This side product occurred upon prolonged light exposure and/or in the presence of a large concentration of RX. Filtering visible light to isolate band gap excitation (λ < 385 nm) of $Co^{III}-R/TiO_2(e^-)$ resulted in generation of more $TiO_2(e^-)$,[38] without measurable changes to

Scheme 2. Summary of the observed mechanism for photogeneration of $Co^{I}/TiO_2(e^-)$, dark reactivity to form $Co^{III}-R/TiO_2$, and $Co^{III}-R/TiO_2(e^-)$, Co^{I}/TiO_2 MLCT excited-state injection, and $Co^{III}-R/TiO_2$ photorelease of R resulting in net $2e^-$-transfer catalysis, when R = benzyl. With 0.2% Py (v/v) or R = hexyl the same catalytic cycle of Co(TCPP) and $TiO_2(e^-)$ intermediates was observed albeit with different rate constants

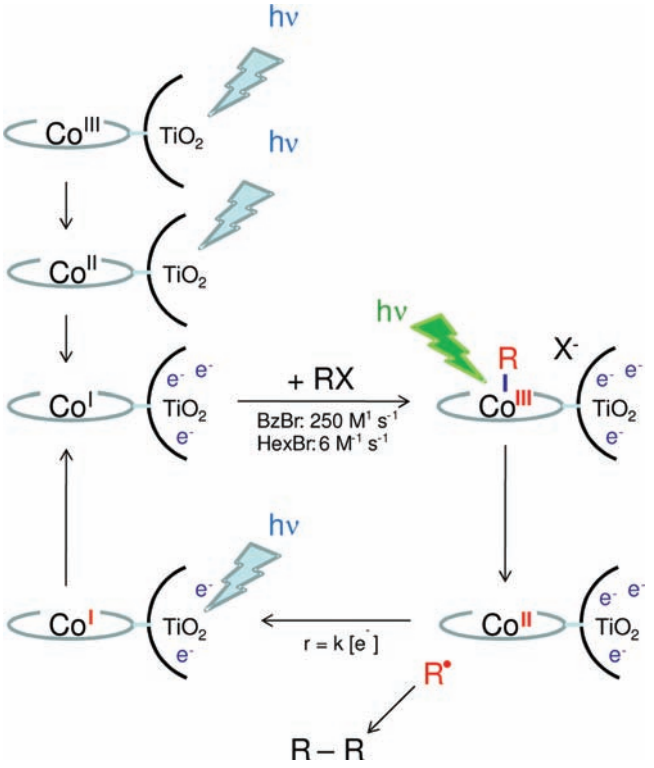

the $Co^{III}-R$ complexes. Thus, TiO_2 served essentially as an electron reservoir for the Co(TCPP) catalyst while wavelength-selective light excitation allowed for control over repopulation of $TiO_2(e^-)$ and/or regeneration of the active state of the metalloporphyrin catalyst.

A sensitized photocurrent was measured when a potentiostatically (−880 mV vs NHE) controlled Co(TCPP)/TiO_2 electrode was illuminated with visible light in the presence of an organobromide. Photocurrent action spectra, plotted as the incident photon-to-current efficiency (IPCE),[21] were in good agreement with the Co^{I}(TCPP)/TiO_2 absorption spectra as shown in Figure 7 for 1-bromohexane. The photocurrent responses achieved steady-state conditions within tens of seconds, Figure 7 inset. By measuring the incoming photon flux and photocurrents, the quantum yield for the catalytic reaction was determined to be 0.03 ± 0.015. Additionally, the turnover frequency for photodissociative photolysis at 410 nm was calculated to be 0.11 ± 0.03 s^{-1}.

■ DISCUSSION

The results presented herein describe new phenomena for two-electron transfer reactions at semiconductor interfaces that are summarized in Scheme 2. Metalloporphyrins were sequentially reduced twice by photo- or electrogenerated semiconductor electrons. The emphasis was on cobalt porphyrins, but similar behavior was observed with hemes. This interfacial redox chemistry was found to be non-Nernstian, and the presence of two well-defined $Co^{III/II}$ and $Co^{II/I}$ electron-transfer reactions have provided new insights into the origin(s) of this behavior. Reactions of the Co^{I} porphyrin with organohalides resulted in oxidative addition $2e^-$-transfer reactivity to form a stable organometallic product that underwent homolytic cleavage of the Co−C bond to yield C−C bonded products when excited with visible light. Nanosecond absorption spectroscopy proved to be a powerful tool for quantifying the mechanisms and yields of the individual steps in the photocatalytic cycle shown. This catalytic cycle was also exploited to generate a photocurrent in an electrosynthetic photoelectrochemical cell. Below we describe details of the two-electron transfer reductions followed by an analysis of the photocatalytic reaction chemistry.

Twice-Reduced Metalloporphyrins. As the quasi-Fermi level of TiO_2 was raised in an electrochemical cell, the metalloporphyrins were reduced from Co^{III} to Co^{II} and then from Co^{II} to Co^{I} formal oxidation states. The assignment of both reductions as formally metal based $Co^{III/II}$ and $Co^{II/I}$ was due to comparison with previously published data.[26−29] The redox chemistry did not follow the Nernst equation and was hence nonideal, often requiring ideality factors greater than 2. Recall that the Nernst equation predicts a factor of 10 change in concentration for every 59 mV, while an ideality factor of 2 would correspond to ∼120 mV. The additional potential energy required for nonideal semiconductor interfaces is significant in solar photocatalysis as more intense band gap illumination is required to maintain a desired redox state or concentration. Furthermore, nonideal behavior raises the question of the true "reduction potential" of the surface-adhered catalyst, with the real possibility that it significantly differs from the solution value. Therefore, understanding the factors that control interfacial nonidealities is important.

The possible origin(s) of nonideal thermodynamic behavior for redox-active molecules in heterogeneous media has been discussed in a recent review.[32,33] Models based on Frumkin isotherms, a Gaussian distribution of reduction potentials, and potential drops across the Helmholtz layer have all been proposed. A novel aspect of the redox chemistry reported herein was that *two* adjacent $Co^{III/II}$ and $Co^{II/I}$ reduction processes were quantified, whereas previous workers quantified only *one*. The availability of two redox processes provided some insights into the factors that control the redox behavior and thus multiple-electron-transfer reactivity at semiconductor interfaces.[12] Specifically, in the presence of hard Lewis acidic Li^+ cations, the TiO_2-mediated $Co^{III/II}$ reduction process was nearly ideal, yet the $Co^{II/I}$ process was not. Such behavior is not easily rationalized with a model wherein intermolecular interactions influence the reduction potentials of catalysts that have not yet been reduced, i.e. Frumkin behavior.[31,39−45] This was further corroborated by the fact that both the ideality factors and the formal reduction potentials were practically independent of the metalloporphyrin surface coverage. Furthermore, while an underlying Gaussian distribution of energetic states may induce a normal distribution of catalyst−semiconductor redox potentials and hence nonunity ideality factors, the data herein would require two very different distributions, and there is no *a priori* reason to suspect that the molecular environment changes significantly in these three formal oxidation states.[32,33,46,47]

The data therefore is most consistent with the fractional potential drop model previously proposed by Gregg, Zaban, and Ferrere.[12] This model predicts a fraction of the electric field

is present across the inner Helmholtz plane at the TiO_2−catalyst interface.[12−14] The observed potential drop is similar to that seen with a parallel-plate capacitor, where the TiO_2 surface and the redox-active portion of the catalysts play the role of the plates. We note that further evidence for electric fields emanating from TiO_2 resulting in potential drops through molecular sensitizers has recently been reported.[48−50] A comparison of the data acquired with tetrabutyl ammonium and lithium cations suggests that ions with high charge-to-size ratios more effectively screen the charge from the catalyst resulting in more ideal behavior. In principle, Li^+, on the basis of its high charge-to-size ratio, could lower the energy required to achieve the catalytic Co^I state. However, for TiO_2, Li^+ shifts the semiconductor acceptor states positive on an electrochemical scale, thereby requiring a higher concentration of $TiO_2(e^-)$ to achieve complete conversion of the metalloporphyrins to their Co^I state. For example, to reduce Co^{II}→Co^I requires almost 3 times the $[TiO_2(e^-)]$ in Li^+ electrolyte relative to tetrabutylammonium electrolyte.

Co^I Reaction Chemistry. The reactivity of $Co^I(TCPP)/TiO_2$ with organobromides was characterized. The reaction of 1-bromohexane or benzyl bromide with $Co^I(TCPP)/TiO_2(e^-)$ resulted in spectral changes consistent with the $2e^-$ transfer, oxidative addition, and formation of Co^{III}−R as a metal−carbon bond, eq 6.[15,16,51]

$$Co^I/TiO_2(e^-) + R-Br \rightarrow Co^{III}-R/TiO_2(e^-) + Br^- \quad (6)$$

The sluggish rate for Co^I reaction with 1-bromohexane, $k_2 \approx 6\ M^{-1}\ s^{-1}$, was increased by over an order of magnitude when benzyl bromide was employed. No measurable reactions were observed in comparative studies with Co^{II}/TiO_2.

Reaction 6 was not catalytic but rather stoichiometric as the organometallic products were stable on the semiconductor surface and effectively prevented further reaction. However, upon visible light photoexcitation of Co^{III}−$R/TiO_2(e^-)$, catalysis was observed. This was confirmed by the appearance of sustained photocurrents after visible-light excitation of Co^{III}−R/TiO_2 thin-film electrodes in photoelectrosynthetic solar cells and by transient absorption spectroscopy where a Co^{II} product was directly observed, consistent with homolytic bond cleavage, Reaction 7.

$$Co^{III}-R/TiO_2(e^-)_n + h\nu_{vis} \rightarrow Co^{II}/TiO_2(e^-)_n + R^{\bullet} \quad (7)$$

In vitamin B_{12} photochemistry, Sension and co-workers have previously shown the initial photoproducts of methylcobalamin photolysis were both Co^{III} and Co^{II}, but only the bond homolysis products avoided rapid geminate recombination (<5 ns).[51,52] As the measurements reported here were conducted on longer time scales, it was not possible to determine whether such a mechanism was also operative. The 0.15 quantum yield measured for homolytic bond cleavage here implies that some sub-nanosecond recombination reactions also occurred consistent with Sension's observations with the biological analogue.[51,52]

The Co^{II} photoproduct was subsequently reduced by the excess electrons present in TiO_2, eq 8.

$$Co^{II}/TiO_2(e^-)_n \rightarrow Co^I/TiO_2(e^-)_{n-1} \quad (8)$$

The kinetics for this reaction were complex but were consistent with those previously measured after excited state injection.[53] It is interesting to note that the Co^{II} to Co^I reduction required milliseconds, even with a driving force near zero. Equation 8 resets the catalyst, and the cycle then repeats, with turnover numbers in the 100s prior to catalyst degradation. Thus, the overall reaction mechanism to form a C−C bond required two catalysts, two RX substrates, two photons, and two $TiO_2(e^-)$'s. At the 0.7 M bromohexane concentrations studied, the rate-limiting step in the catalytic cycle was oxidative addition to Co^ITCPP, with turnover frequencies on the order of $1\ s^{-1}$ calculated from transient absorption experiments. The turnover frequency abstracted from photocurrent measurements was $0.11 \pm 0.03\ s^{-1}$, in reasonable agreement with the transient data noting the inherent differences in the experiments. Previous researchers have considered the turnover frequency required for a catalyst to produce the maximum amount of fuel under 1 sun (100 mW/cm^2) of solar irradiation. Frei concluded that a solar catalyst must have a turnover frequency in excess of 100 $s^{-1}\ nm^{-2}$ to match the solar flux.[54] The metalloporphyrin catalysts are roughly 1 nm^2, and in principle, the mesoporous films afford a 1000-fold increase in the surface area over a planar electrode. Therefore, when anchored to high surface area supports, the measured turnover frequencies of these metalloporphyrins are close to correct for solar photocatalysis.

CONCLUSIONS

Herein we have shown that metalloporphyrins anchored to mesoporous, nanocrystalline TiO_2 thin-film electrodes can be reduced from their native M^{III} redox states to M^I via two sequential reductions, albeit with nonideal redox behavior. The elongated range of potentials over which each reduction was observed was unexpected on the basis of first principles thermodynamics, yet could be reasonably explained by a mechanism whereby an electric field and potential drop across the molecule−semiconductor interface was present. Addition of organohalides to $Co^I(TCPP)/TiO_2$ resulted in oxidative addition reactions that form stable organometallic compounds. Visible-light excitation of the organometallic compound resulted in prompt photorelease of $R^{\bullet}$ that couples to form bibenzyl, when R = benzyl.[55,56] After subsequent reduction of Co^{II} to Co^I by $TiO_2(e^-)$ over the micro- to millisecond time scale, the catalytic cycle was complete via reaction with another organohalide in fluid solution. The utility of employing cobalt-based coordination compounds for multiple-electron-transfer reactivity has implications for the feasibility of large-scale direct solar fuel-forming systems. The strategy of using short wavelengths of light to directly excite the semiconductor and longer wavelengths to cleave metal−carbon bonds was successful. The present work required methanol as a sacrificial reagent to consume valence band holes that could in principle be eliminated in tandem solar cell configurations.

ASSOCIATED CONTENT

Supporting Information. Chemical capacitance analysis for $Fe(PPIX)/TiO_2$. This material is available free of charge via the Internet at http://pubs.acs.org.

AUTHOR INFORMATION

Corresponding Author
meyer@jhu.edu

■ ACKNOWLEDGMENT

We acknowledge support by a grant from the National Science Foundation (091158). S.A. acknowledges a Johns Hopkins University Greer graduate student fellowship. M.A. thanks the Swedish Research Council for a personal postdoctoral research grant, 623-2007-1038.

■ REFERENCES

(1) Fujishima, A.; Honda, K. *Nature* **1972**, *238*, 37–38.
(2) Nozik, A. J. *Nature* **1975**, *257*, 383–386.
(3) Wrighton, M. S.; Ginley, D. S.; Wolczanski, P. T.; Ellis, A. B.; Morse, D. L.; Linz, A. *Proc. Natl. Acad. Sci. U.S.A.* **1975**, *72*, 1518–1522.
(4) Wrighton, M. S.; Ellis, A. B.; Wolczanski, P. T.; Morse, D. L.; Abrahamson, H. B.; Ginley, D. S. *J. Am. Chem. Soc.* **1976**, *98*, 2774–2779.
(5) Khaselev, O.; Turner, J. A. *Science* **1998**, *280*, 425–427.
(6) Kanan, M. W.; Nocera, D. G. *Science* **2008**, *321*, 1072–1075.
(7) Bard, A. J.; Fox, M. A. *Acc. Chem. Res.* **1995**, *28*, 141–145.
(8) Mamedov, A. A.; Belov, A.; Giersig, M.; Mamedova, N. N.; Kotov, N. A. *J. Am. Chem. Soc.* **2001**, *123*, 7738–7739.
(9) Kamat, P. V. *J. Phys. Chem. C* **2008**, *112*, 18737–18753.
(10) Kongkanand, A.; Tvrdy, K.; Takechi, K.; Kuno, M.; Kamat, P. V. *J. Am. Chem. Soc.* **2008**, *130*, 4007–4015.
(11) Shankar, K.; Basham, J. I.; Allam, N. K.; Varghese, O. K.; Mor, G. K.; Feng, X.; Paulose, M.; Seabold, J. A.; Choi, K.-S.; Grimes, C. A. *J. Phys. Chem. C* **2009**, *113*, 6327–6359.
(12) Zaban, A.; Ferrere, S.; Sprague, J.; Gregg, B. A. *J. Phys. Chem. B* **1997**, *101*, 55–57.
(13) Zaban, A.; Ferrere, S.; Gregg, B. A. *J. Phys. Chem. B* **1998**, *102*, 452–460.
(14) Gregg, B. A. *Coord. Chem. Rev.* **2004**, *248*, 1215–1224.
(15) Lexa, D.; Saveant, J. M.; Soufflet, J. P. *J. Electroanal. Chem.* **1979**, *100*, 159–172.
(16) Fritsch, J. M.; McNeill, K. *Inorg. Chem.* **2005**, *44*, 4852–4861.
(17) Qiu, A.; Sawyer, D. T. *J. Porphyrins Phthalocyanines* **1997**, *1*, 125–134.
(18) Obare, S. O.; Ito, T.; Meyer, G. J. *Environ. Sci. Technol.* **2005**, *39*, 6266–6272.
(19) Obare, S. O.; Ito, T.; Meyer, G. J. *J. Am. Chem. Soc.* **2006**, *128*, 712–713.
(20) Stromberg, J. R.; Wnuk, J. D.; Pinlac, R. A. F.; Meyer, G. J. *Nano Lett.* **2006**, *6*, 1284–1286.
(21) O'Regan, B. C.; Durrant, J. R. *Acc. Chem. Res.* **2009**, *42*, 1799–1808.
(22) Heimer, T. A.; D'Arcangelis, S. T.; Farzad, F.; Stipkala, J. M.; Meyer, G. J. *Inorg. Chem.* **1996**, *35*, 5319–5324.
(23) Trammell, S. A.; Meyer, T. J. *J. Phys. Chem. B* **1999**, *103*, 104–107.
(24) Argazzi, R.; Bignozzi, C. A.; Heimer, T. A.; Castellano, F. N.; Meyer, G. J. *Inorg. Chem.* **1994**, *33*, 5741–5749.
(25) Bard, A. J.; Faulkner, L. R. *Electrochemical Methods: Fundamentals and Applications*, 2nd ed.; John Wiley & Sons, Inc.: New York, 2001.
(26) Rothenberger, G.; Fitzmaurice, D.; Grätzel, M. *J. Phys. Chem.* **1992**, *96*, 5983–5986.
(27) Boschloo, G.; Fitzmaurice, D. *J. Phys. Chem. B* **1999**, *103*, 7860–7868.
(28) Boschloo, G.; Fitzmaurice, D. *J. Phys. Chem. B* **1999**, *103*, 2228–2231.
(29) Felton, R. H.; Linschitz, H. *J. Am. Chem. Soc.* **1966**, *88*, 1113–1116.
(30) Balch, A. L.; Noll, B. C.; Olmstead, M. M.; Phillips, S. L. *Inorg. Chem.* **1996**, *35*, 6495–6506.
(31) Chidsey, C. E. D.; Murray, R. W. *J. Phys. Chem.* **1986**, *90*, 1479–1484.
(32) Bisquert, J.; Garcia-Belmonte, G.; García-Cañadas, J. *J. Chem. Phys.* **2004**, *120*, 6726–6733.
(33) Bisquert, J.; Fabregat-Santiago, F.; Mora-Sero, I.; Garcia-Belmonte, G.; Barea, E. M.; Palomares, E. *Inorg. Chim. Acta* **2008**, *361*, 684–698.
(34) Williams, G.; Watts, D. C. *Trans. Faraday Soc.* **1970**, *66*, 80–85.
(35) Lindsey, C. P.; Patterson, G. D. *J. Chem. Phys.* **1980**, *73*, 3348–3357.
(36) Xia, H.-L.; Ardo, S.; Narducci Sarjeant, A. A.; Huang, S.; Meyer, G. J. *Langmuir* **2009**, *25*, 13641–13652.
(37) Zheng, G. D.; Yan, Y.; Gao, S.; Tong, S. L.; Gao, D.; Zhen, K. J. *Electrochim. Acta* **1996**, *41*, 177–182.
(38) Green, A. N. M.; Chandler, R. E.; Haque, S. A.; Nelson, J.; Durrant, J. R. *J. Phys. Chem. B* **2005**, *109*, 142–150.
(39) Laviron, E. *Electroanal. Chem. Interfacial Electrochem.* **1974**, *52*, 395–402.
(40) Laviron, E. *J. Electroanal. Chem.* **1975**, *63*, 245–261.
(41) Brown, A. P. *Anal. Chem.* **1977**, *49*, 1589–1595.
(42) Smith, D. F.; Willman, K.; Kuo, K.; Murray, R. W. *J. Electroanal. Chem.* **1979**, *95*, 217–227.
(43) Ellis, D.; Eckhoff, M.; Neff, V. D. *J. Phys. Chem.* **1981**, *85*, 1225–1231.
(44) Laviron, E. *J. Electroanal. Chem.* **1981**, *122*, 37–44.
(45) Ikeda, T.; Leidner, C. R.; Murray, R. W. *J. Electroanal. Chem.* **1982**, *138*, 343–365.
(46) Albery, W. J.; Boutelle, M. G.; Colby, P. J.; Hillman, A. R. *J. Electroanal. Chem.* **1982**, *133*, 135–145.
(47) Albery, W. J.; Bartlett, P. N.; Wilde, C. P.; Darwent, J. R. *J. Am. Chem. Soc.* **1985**, *107*, 1854–1858.
(48) Staniszewski, A.; Ardo, S.; Sun, Y.; Castellano, F. N.; Meyer, G. J. *J. Am. Chem. Soc.* **2008**, *130*, 11586–11587.
(49) Ardo, S.; Sun, Y.; Castellano, F. N.; Meyer, G. J. *J. Phys. Chem. B* **2010**, *114*, 14596–14604.
(50) Ardo, S.; Sun, Y.; Staniszewski, A.; Castellano, F. N.; Meyer, G. J. *J. Am. Chem. Soc.* **2010**, *132*, 6696–6709.
(51) Walker, L. A.; Jarrett, J. T.; Anderson, N. A.; Pullen, S. H.; Matthews, R. G.; Sension, R. J. *J. Am. Chem. Soc.* **1998**, *120*, 3597–3603.
(52) Shiang, J. J.; Walker, L. A.; Anderson, N. A.; Cole, A. G.; Sension, R. J. *J. Phys. Chem. B* **1999**, *103*, 10532–10539.
(53) Achey, D.; Ardo, S.; Xia, H.; Siegler, M. A.; Meyer, G. J. *J. Phys. Chem. Lett.* **2011**, *2*, 305–308.
(54) Jiao, F.; Frei, H. *Angew. Chem., Int. Ed.* **2009**, *48*, 1841–1844.
(55) Isse, A. A.; Gennaro, A. *Indian J. Chem., Sect. A: Inorg., Bio-inorg., Phys., Theor. Anal. Chem.* **2003**, *42*, 751–757.
(56) Isse, A. A.; De Giusti, A.; Gennaro, A. *Tetrahedron Lett.* **2006**, *47*, 7735–7739.